HHS Public Access

Author manuscript

Pacing Clin Electrophysiol. Author manuscript; available in PMC 2021 June 17.

Published in final edited form as:

Pacing Clin Electrophysiol. 2021 March ; 44(3): 432–441. doi:10.1111/pace.14181.

Feasibility study shows concordance between image-based virtual-heart ablation targets and predicted ECG-based arrhythmia exit-sites

Shijie Zhou, PhD[#1,5], **Eric Sung, BA**[#1,5], **Adityo Prakosa, PhD**[1,5], **Konstantinos N. Aronis, MD**[2,5], **Jonathan Chrispin, MD**[2,5], **Harikrishna Tandri, MD**[2,5], **Amir AbdelWahab, MD**[3], **B. Milan Horáček, PhD**[4], **John L. Sapp, MD**[3], **Natalia A. Trayanova, PhD**[1,5]

[1]Department of Biomedical Engineering, Johns Hopkins University, Baltimore, Maryland, USA

[2]Section of Cardiac Electrophysiology, Division of Cardiology, Department of Medicine, Johns Hopkins Hospital, Baltimore, Maryland, USA

[3]Department of Medicine, Queen Elizabeth II Health Sciences Centre, Halifax, Nova Scotia, Canada

[4]School of Biomedical Engineering, Dalhousie University, Halifax, Nova Scotia, Canada

[5]Alliance for Cardiovascular Diagnostic and Treatment Innovation, Johns Hopkins University, Baltimore, Maryland, USA

[#] These authors contributed equally to this work.

Abstract

Introduction: We recently developed two noninvasive methodologies to help guide VT ablation: population-derived automated VT exit localization (PAVEL) and virtual-heart arrhythmia ablation targeting (VAAT). We hypothesized that while very different in their nature, limitations, and type of ablation targets (substrate-based vs. clinical VT), the image-based VAAT and the ECG-based PAVEL technologies would be spatially concordant in their predictions.

Objective: The objective is to test this hypothesis in ischemic cardiomyopathy patients in a retrospective feasibility study.

Methods: Four post-infarct patients who underwent LV VT ablation and had pre-procedural LGE-CMRs were enrolled. Virtual hearts with patient-specific scar and border zone identified potential VTs and ablation targets. Patient-specific PAVEL based on a population-derived

Correspondence: Natalia A. Trayanova, PhD, Department of Biomedical Engineering, Johns Hopkins University, Baltimore, MD, USA. ntrayanova@jhu.edu.

CONFLICTS OF INTEREST

Dr. B. Milan Horáček: a co-holder of a patent for automated VT localization; no licensing, royalties or income currently or anticipated. Dr. Amir AbdelWahab: speaker honoraria Abbott, Medtronic. Dr. John L. Sapp: a co-holder of a patent for automated VT localization; no licensing, royalties or income currently or anticipated. Research funding from Biosense-Webster and Abbott (for clinical trial of catheter ablation of VT); modest speaker honoraria Medtronic, Biosense Webster, Abbott. Dr. Trayanova partial ownership CardioSolv LLC.

SUPPORTING INFORMATION

Additional supporting information may be found online in the Supporting Information section at the end of the article.

statistical method localized VT exit sites onto a patient-specific 238-triangle LV endocardial surface.

Results: Ten induced VTs were analyzed and 9-exit sites were localized by PAVEL onto the patient-specific LV endocardial surface. All nine predicted VT exit sites were in the scar border zone defined by voltage mapping and spatially correlated with successful clinical lesions. There were 2.3 ± 1.9 VTs per patient in the models. All five VAAT lesions fell within regions ablated clinically. VAAT targets correlated well with 6 PAVEL-predicted VT exit sites. The distance between the center of the predicted VT-exit-site triangle and nearest corresponding VAAT ablation lesion was 10.7 ± 7.3 mm.

Conclusions: VAAT targets are concordant with the patient-specific PAVEL-predicted VT exit sites. These findings support investigation into combining these two complementary technologies as a noninvasive, clinical tool for targeting clinically induced VTs and regions likely to harbor potential VTs.

Keywords

ECG; ischemic cardiomyopathy; late gadolinium-enhanced cardiac magnetic resonance imaging; radiofrequency (RF) ablation; ventricular tachycardia

1 | INTRODUCTION

Ventricular tachycardia (VT), a life-threatening fast heart rhythm, frequently occurs in patients with prior myocardial infarction (MI), leading to sudden cardiac death (SCD).[1] Catheter ablation has become an evidenced therapeutic option for the treatment of VTs[2] for patients with prior myocardial infarction (MI) and recurrent VT.[3] Despite its importance, it continues to be a challenging procedure in clinical electrophysiology. The majority of infarct-related VTs are poorly hemodynamically tolerated, may be difficult to induce, and frequently transform to other tachycardias during catheter mapping.[4] Three-dimensional (3D) substrate mapping has added substantial capability and insight into catheter ablation of VT,[5–7] but the procedure is restricted by the limitations of point-by-point catheter mapping, even with newer multipolar catheter rapid mapping techniques.[7] Thus, there is an urgent need to precisely characterize the arrhythmogenic substrate for infarct-related VTs.

We recently developed two independent noninvasive methodologies to help guide VT ablation: the population-derived automated VT exit localization (PAVEL)[8] and the virtual-heart arrhythmia ablation targeting (VAAT).[9] Using a population-derived statistical estimates, PAVEL noninvasively localizes VT exit sites onto one of 238 triangular elements of a generic left ventricular (LV) endocardial surface using eight independent leads (I, II, V1-V6) of the standard 12-lead ECG.[8] PAVEL's ability to localize VT exit sites was prospectively assessed in patients with scar-related VT, achieving a promising mean localization accuracy 9.5 ± 2.6 mm.[10] However, while PAVEL predictions are based on information from the ECG, the methodology does not incorporate any information about the patient-specific heart geometry or infarct scar distribution.

VAAT is a noninvasive personalized ablation targeting approach based on imaging and computational modeling. It entails constructing geometrical models of the patient's

ventricles from late gadolinium-enhanced cardiac magnetic resonance imaging (LGE-CMR) thus representing the patient-specific ventricular geometry and scar and infarct border zone distributions. It assigns different electrophysiological properties in the different regions in the remodeled ventricles. Simulating the response of the ventricles to rapid pacing from a large number of sites, VAAT determines the locations, in the remodeled substrate, of highest propensity to VT occurrence, that is, the VAAT targets. VAAT-predicted targets have been demonstrated to be consistent with clinical ablation lesions in a retrospective study, and to achieve acute VT termination in a small multicenter prospective study.[9] However, VAAT's predictions do not incorporate patient-specific electrophysiological information, which could be gleaned from the 12-lead ECG, a tool of unparalleled importance in ablation procedures.[11]

We hypothesized that while very different in their nature, limitations, and type of ablation targets (substrate-based vs. clinical VT), the image-based VAAT and the ECG-based PAVEL technologies would nonetheless be spatially concordant in predictions when appropriate. The goal of this study is to test this hypothesis. Establishing this relationship is significant because both techniques are noninvasive, provide complementary information, and are applicable to both hemodynamically stable and unstable VTs. Thus, if the predictions are consistent, there could be potential for combining them into a unified pre-procedural technology to inform a comprehensive ablation strategy.

2 | METHODS

2.1 | Study population

Four patients with ischemic cardiomyopathy (ICM) who underwent LV endocardial VT ablation were included in this retrospective study. This study was approved by the Institutional Review Board (IRB) at the Johns Hopkins Hospital, and all patients gave written informed consent.

2.2 | Clinical electrophysiology (EP) mapping and catheter ablation

Catheter ablation of infarct-related VT was performed using standard techniques.[7] VT was induced by programmed ventricular stimulation from the right ventricular (RV) apex or outflow tract. Access to the LV was achieved via a retrograde aortic or trans-septal approach. For each procedure, Carto 3 (Biosense Webster, Diamond Bar, CA) system was used for electroanatomic mapping (EAM); an EAM was created using an open-irrigated catheter (ThermoCool SmartTouch, Biosense Webster, Diamond Bar, CA) or a multi-electrode catheter (PentaRay NAV Catheter, Biosense Webster). Substrate-based mapping and pace-mapping were used to identify scar and potential culprit sites within the scar, which were targeted for ablation. Radiofrequency (RF) ablation was performed using an open-irrigated catheter (ThermoCool Smart-Touch., Biosense Webster, Diamond Bar, CA) when targeting the critical isthmus and areas of late potentials.

2.3 | LGE-CMR acquisition

LGE-CMR images acquired using 1.5-T cardiac magnetic resonance scanner (Avanto; Siemens, Erlangen, Germany) were utilized to reconstruct the ventricular geometry and

distributions of scar and grey zone. Scans were performed 15 min after intravenous administration of 0.2 mmol/kg gadopentetate dimeglumine. LGE-CMR images were obtained in a short axis with a segmented inversion recovery gradient echo turbo-fast low-angle shot sequence (echo time 1.3–3.9 ms, repetition time 5.4–8.3 ms, average in-plane resolution 1.5×1.5 mm, 8-mm slice thickness) (Figure 1, panel A). The inversion time was modified iteratively to maximize the conspicuity of myocardial areas with delayed enhancement.

2.4 | ECG acquisition and processing

For the retrospective study, digitized 12-lead ECG signals of induced VTs of each patient were acquired from the Prucka CardioLab electrophysiology system (GE Healthcare, Waukesha, WI) for offline analysis. The digitized 12-lead ECG signals were band-pass filtered 0.05–100 Hz, with 60 Hz notch filter and sampled at 977 Hz. Within each induced and mapped VT, a VT beat was manually selected for analysis. We used QRS integrals (∫QRS) to reduce ECG data to one variable per lead. The values of the 120-ms ∫QRS from the eight independent ECG leads (I, II, V1-V6) of the VT ECG are calculated.[8] The QRS onset was automatically identified.[12] The 120-ms window could be manually adjusted in the PAVEL approach if correction of QRS onset was necessary.

2.5 | Ablation procedure data

EAM data and ablation lesion locations were acquired for all patients. For comparison between the patient-specific PAVEL and VAAT predictions, EAM bipolar potential maps and clinical ablation locations were registered to the virtual hearts and the 238-triangle patient-specific LV endocardial surfaces using the same registration process as previously described.[9]

2.6 | VAAT methodology

A full description of the personalized VAAT workflow can be found in our previous publication.[9] Briefly, three-dimensional (3D) ventricular models of the post-infarct LV were reconstructed from the segmented myocardium along with the patients' distributions of scar grey zone and normal myocardial tissues (Figure 1, panel B).[13,14] To execute numerical simulations, finite-element ventricular meshes were generated as described previously.[14] Myocardial fiber orientations were assigned using a validated rule-based approach.[15] Electrophysiological properties were assigned to the three regions outlined in the virtual heart from the LGE-CMR images: scar, grey zone, and normal myocardial tissue.[14] The scar tissue was assigned to be electrically insulating. Normal myocardium and grey zone region electrophysiological properties were assigned the same as in previous works.[9]

The response of each personalized post-infarction ventricular model to rapid pacing from a large number of sites was next evaluated to determine the locations of propensity to VT occurrence.[14] For each location of propensity to VT occurrence (Figure 1, panel C),VAAT ablation lesions were applied to either the entrance, isthmus, or exit site of the induced VT at that location (depending on the structure of the surrounding scar and grey zone and aiming at a with minimum lesion size). Targeting in this manner, all ventricular locations of VT occurrence propensity render the personalized virtual heart noninducible for VT from any

pacing location (Figure 1, panel D). Unlike substrate modification strategies that involve empirically targeting electrophysiological abnormalities, VAAT is a "focused substrate-based" ablation strategy that targets only regions predicted to harbor VT circuits. It is important to note that VAAT predicts ablation targets only arising from the structurally remodeled substrate (scar of infarct border zone—in case there is no enhancement on the CMR for a given patient, VAAT would not be the appropriate ablation guidance approach. Because new VTs could arise post-ablation, the new modified substrate arrhythmogenicity was re-assessed to comprehensively identify all possible clinical and nonclinical VT morphologies that the substrate could harbor.

2.7 | PAVEL methodology

Details about the PAVEL algorithm can be found in our prior publication.[8,16] Briefly, a generic LV endocardial surface with 238 triangular area elements was obtained from the necropsy specimen of a normal human heart.[17] The PAVEL system combines information from an acquired eight-lead ECGs (leads I, II, V1-V6) of an induced VT and population-derived regression coefficients to identify the site of earlies LV activation onto the generic LV endocardial surface. A total of 1012 pacing sites, each of which were manually registered onto one of 238 triangles whose coordinate centers of the generic LV endocardial surface and their corresponding eight-lead ECGs, constituted a training set for computing population-derived regression coefficients.[8,16] For the acquired ECG of the induced VT, the PAVEL system calculates the 120-ms $\int$QRS of eight leads (Figure 1, panel E), and uses the population-derived regression coefficients determined in a multiple regression model to predict the VT exit site coordinates (x, y, z) from the eight-lead 120-ms $\int$QRS of the VT. The predicted VT exit site coordinates (x, y, z) are projected onto one of the generic LV's 238 triangular area elements using a nearest neighbor algorithm, so that the location can be targeted as a predicted VT exit site (Figure 1, panel F). It is important to note that PAVEL predicts VT exit sites but does not yield information about the substrate, the structure of the VT, or where to ablate.

2.8 | Altering PAVEL to incorporate the patient-specific LV endocardial surface

To be able to better compare PAVEL-predicted VT exit sites with VAAT ablation targets, we projected the generic LV 238-triangle surface mesh onto each patient-specific LV endocardial surface (Figure 1, panel G). A schematic of how this was done is shown in Figure S1.

2.9 | Analysis

The locations of VAAT targets were compared to the locations of the patient-specific PAVEL-predicted VT exit sites. As VAAT targets all potential locations of VT propensity as a focused structural-remodeling substrate-based ablation strategy, the targeted locations may or may not correspond to locations of clinical VTs. On the other hand, PAVEL predicts the exit sites only for VT induced in the patient. Thus, if a VAAT target would correspond to a clinical VT, then it would also be expected that it will be spatially concordant with the PAVEL-predicted exit site for that VT. Accordingly, only VAAT target locations that were located proximal to the PAVEL-predicted VT exit sites were examined. To quantitatively assess how such VAAT targets spatially correlated with PAVEL VT exit sites, the minimum

distance between the center of the PAVEL-predicted exit site triangles and the nearest VAAT target was computed. It is important to note that even in the case of perfect correspondence between a clinical VT and a VT induced in the model, the VAAT target could be at a distance from the PAVEL VT exit site, as the VAAT algorithm might have found most suitable to create a lesion in the middle of a conducting channel, for instance.

3 | RESULTS

3.1 | Patients

We retrospectively enrolled 4 patients who underwent LV endocardial VT ablation and had pre-procedural 2D LGE-CMR. The patients' clinical variables are described in Table 1. Ten VTs were induced across the four patients.

3.2 | Patient-specific PAVEL VT exit site predictions

Table 2 lists each patient-specific LV endocardial surface with the corresponding number of triangular elements. Three out of four patients did not have the complete LV base visible on the 2D LGE-MRI; thus, the patient-specific LV endocardial surface did not include the basal triangular elements for these three patients (total of 36 triangular elements not included). The mean area of all the triangular elements for the four patient-specific LV endocardial surfaces was 0.79 ± 0.16 cm^2 (mean ± SD). Nine out of 10 VT exit sites were localized by PAVEL onto the patient-specific LV endocardial surfaces; one VT exit site for patient 4 was too basal to be localized onto the patient-specific LV endocardial surface. The mean area of the triangular elements onto which the nine predicted VT exit sites were localized was 0.75 ± 0.23 cm^2 (mean ± SD). Figure 2 shows the nine VT exit sites predicted by the patient-specific PAVEL and the corresponding 12-lead ECGs of the VTs. All nine predicted VT exit sites were located in the scar border zone defined by substrate voltage mapping and spatially correlated with the successful ablation lesions (Figure 2, left column). These results suggest that the patient-specific PAVEL predictions were consistent with the clinically-observed VT morphologies targeted during the procedure.

3.3 | Spatial concordance between virtual-heart VT circuits and PAVEL-predicted VT exit sites

There were 2.3 ± 1.9 VTs induced on average per virtual heart (Table 2). Figure 3 shows the comparison between PAVEL-predicted VT exit sites and the closest corresponding locations of the VAAT targets.

Patient #1: PAVEL-predicted VT exit sites A and C were in the apical anteroseptal region, and the triangles to which they belonged were directly adjacent to one another, suggesting that they shared a conduction channel and thus potentially belonged to the same VT. Both exit sites A and C co-localized with the exit site of a VT circuit induced in the corresponding virtual heart. The PAVEL-predicted VT exit site B was located adjacent to an area of border zone as defined on bipolar voltage mapping, however, there was no scar or grey zone identifiable on LGE-MRI in that region (Figure S2), which explains why there was no substrate-based VT in the virtual heart at that location.

Patient #2: The patient had only one inducible VT during the ablation procedure. The PAVEL-predicted VT exit site was located in the basal lateral wall at the scar margin and correlated with the exit site of one of five virtual-heart VT re-entrant circuits, indicating that this was clinical VT. The virtual heart approach predicted another four substrate-based locations that could harbor VT circuits. These were located along the margins of the scar on the lateral and inferolateral LV walls and co-localized with a cluster of clinical substrate-modification ablation lesions.

Patient #3: There were three induced VTs during the ablation procedure. Two virtual-heart VTs clearly manifested on the epicardial surface. One virtual-heart VT localized to the mid inferior wall of the LV; its exit site matched the PAVEL-predicted VT exit site A, and its entrance site matched the PAVEL-predicted VT exit site C (Figure 3, top right). This implies that the VT morphologies corresponding to exit sites A and C shared a common conduction channel. The second virtual-heart VTs localized to the mid infero-septum and its exit site closely correlated with PAVEL's predicted VT exit site B.

Patient #4: Two VTs were induced in the clinic. The PAVEL-predicted VT exit site B was located on the apical inferolateral wall of the LV and co-localized with the exit site of a virtual-heart VT. PAVEL-predicted VT exit site A was located in the basal lateral wall. However, this region was obscured by ICD artifact and could not be represented as remodeled in the virtual heart, thus there were no VAAT predictions at that location.

3.4 | Comparison between VAAT targets and PAVEL-predicted VT exit sites

All VAAT ablation lesions for the four patients fell within regions ablated clinically. Table 2 lists computed distances from the PAVEL-predicted VT exit site to the nearest VAAT ablation lesion. Overall, the mean distance between the center of the PAVEL-predicted VT exit site triangle and the nearest corresponding VAAT ablation lesion was 10.7 ± 7.3 mm (Table 2).

Figure 4 illustrates the relationship between the VAAT targets and the patient-specific PAVEL VT exit site predictions for each patient along with the corresponding substrate voltage maps. For four VTs (patient 1 VT A and C, patient 3 VT A and B), PAVEL predicted VT exit sites overlapped with the VAAT targets (Figure 4, left column). For patient 1 VT A and C, the VAAT-predicted targets were directly adjacent to the PAVEL-predicted VT exit sites along the border zone of the apical infarct (Figure 4 right column, row 1). For patient 3, the VAAT targets were in the mid inferior and mid inferoseptal regions, aligning directly with the VT exit sites for VT A and B. Thus, these results indicate that the VAAT algorithm targeted the exit sites for these 4 VT circuits.

For the remaining two VTs (patient 2 VT A, patient 4 VT B), the PAVEL-predicted VT exit sites were located close (less than 20 mm) to the VAAT ablation lesions (Figure 4, left column). These two VTs were terminated within the middle of the low-voltage scar at sites proximal to the exit. The VAAT targets overlapped with the clinical ablation lesions (Figure 4). The PAVEL-predicted VT exit sites were located in the border zone (Figure 4, right column). This suggests that there was a conducting channel connecting the location of the VAAT target and the PAVEL-predicted VT exit site.

4 | DISCUSSION

The present retrospective feasibility study demonstrated that in patients with ischemic cardiomyopathy, the blindly-predicted VAAT targets are concordant with the VT exit sites determined by the patient-specific PAVEL system. These results highlight the complementary nature of these two non-invasive technologies and the potential for them to be combined for prospective use.

VAAT is a targeted substrate modification, identifying all possible locations in the remodeled substrate that can sustain VT. VAAT relies on personalized image-based data regarding the structural remodeling in the ventricles but does not capitalize on information gained from the 12-lead ECG. It is also unknown which VAAT-predicted targets correspond to clinically induced VT morphologies. In contrast, PAVEL performs VT exit site localization using the 12-lead ECGs of clinically-induced VTs. PAVEL, however, is a substrate-agnostic approach and alone does not indicate where ablation lesions should be delivered. Hence, even while using PAVEL, it is still necessary to create a dense high-resolution substrate map in order to understand the clinically-induced VT circuits to subsequently determine the appropriate ablation targets. Thus, the combination of PAVEL and VAAT would overcome their respective disadvantages. It would yield a noninvasive technology that provides a detailed ablation plan for targeting clinically-inducible VT morphologies as well as for anticipating the outcome of index ablation and adjusting the ultimate ablation target set to account for potential locations in the substrate of high propensity to VT formation.

We envision that the combined PAVEL and VAAT technology would allow for a real-time, hierarchical ablation strategy based on the patient-specific substrate that could be used for both hemodynamically stable and unstable clinically induced VTs. First, VAAT would be computed and exported to the EAM navigation system[9] where VAAT-predicted targets would be displayed on the patient-specific LV geometry. PAVEL's VT exit site predictions are in real time.[10] Then, ablation at the VAAT targets corresponding to clinically induced VT morphologies (as identified by PAVEL's VT exit site localization) could be delivered. Furthermore, VAAT targets not corresponding to the induced VTs would represent recommended ablation regions that could harbor VTs; the delivery of these recommended targets would be left up to the discretion of the clinical team. Thus, this stratified approach would aid clinicians in personalizing an ablation strategy that targets regions sustaining clinically-induced VTs, suggest ablation regions likely to harbor VTs and assesses the arrhythmogenicity of post-ablation substrate by repeating the VAAT protocol. Implementation of this technology could decrease the need for extensive, high-resolution electroanatomic maps which would decrease procedural time and potential radiation exposure from fluoroscopy. Further prospective studies will need to be performed to fully explore the capabilities of a combined VAAT and PAVEL system. In addition, both VAAT and PAVEL are non-invasive, a combined technology could also be a useful adjunct in pre-procedural planning for non-invasive stereotactic radiation ablation.[18]

Overall, the distances between PAVEL exit sites and VAAT ablations for patients 2, 3, and 4 ranged from 13 to 19 mm. As we emphasized in Methods, an overlap between PAVEL-

predicted VT exit sites and VAAT ablations was not expected, as the VAAT algorithm does not necessarily target VT exit sites. The VAAT targets are the locations in the scar/grey zone that are most likely to sustain VT, and thus they are typically part of the critical isthmus of the clinically-induced VT circuit. Although the VAAT lesions were > 15mm away from the VT exit sites in patients 2 and 4, these could still be consistent with the clinical VT circuit since the length of the conducting channel could be as long as 32 mm.[19] In addition, the accuracy of PAVEL could contribute an error to VT exit site localization. PAVEL has been shown to localize the 3D coordinates of a pacing site on the LV endocardium with an accuracy of 12.5 mm.[16] This error was for localizing a pacing site and not a VT exit site; in the latter case, we expect a higher margin of error. For patient 3, there was an average of 13.1 mm distance between the patient-specific PAVEL-predicted VT exit site and the VAAT-predicted target, which is close to reported localization error.

4.1 | Limitations

There are several limitations to this retrospective study. First, this study lacks clinically-identified VT exit sites, meaning that we could not quantify the error between the patient-specific PAVEL-predicted VT exit sites and a clinical reference. However, given that the generic PAVEL was previously validated prospectively with promising localization accuracy within 10 mm,[8] we would expect the localization error to be small because of the only difference between the two PAVEL approaches was in the LV endocardial surface (patient-specific vs. and generic). A future study will need to be performed to quantify localization errors of the patient-specific PAVEL approach. Second, this retrospective study size is small. While these findings are promising, the clinical utility of combining these two methodologies will need to be further explored in larger studies. Third, the patient-specific geometries were reconstructed from the low-resolution 2D LGE-CMR images, which resulted in incomplete geometric reconstructions with part of the LV base missing. Further studies should overcome this limitation by using 3D LGE-CMR to obtain complete whole-heart geometries. Fourth, LGE-CMR ICD artifacts present in patients could disrupt image quality and affect the image processing of scar and grey zone. Although additional steps were taken to overcome the presence of artifacts in the image,[9] it is possible that residual artifact remained. Lastly, both methodologies were developed and performed for the LV chamber. The applicability of both techniques to the RV endocardium is yet to be established but should also be further explored.

5 | CONCLUSIONS

This study demonstrated that in patients with ischemic cardiomyopathy, ablation targets predicted by the VAAT approach are concordant with VT exit sites predicted by the patient-specific PAVEL system. Overall, these findings support further assessment and investigation into combining these two complementary technologies as a noninvasive, clinical tool for targeting of clinically induced VTs and regions likely to harbor potential VTs, including those that could support arrhythmogenesis post-initial ablation.

Supplementary Material

Refer to Web version on PubMed Central for supplementary material.

ACKNOWLEDGMENTS

This work was supported by funding support from the Heart Rhythm Society Postdoctoral Fellowship to S.Z.; NIH [R01HL142496 and R01HL126802] to N.T., Leducq 16CVD02 to N.T.

DATA AVAILABILITY STATEMENT

The data are available from the corresponding author on reasonable request.

REFERENCES

1. Koplan BA, Stevenson WG. Ventricular tachycardia and sudden cardiac death. Mayo Clin Proc. 2009;84:289–297. [PubMed: 19252119]
2. Stevenson WG, Tedrow UB, Reddy V, et al. Infusion needle radiofrequency ablation for treatment of refractory ventricular arrhythmias. J Am Coll Cardiol. 2019;73:1413–1425. [PubMed: 30922472]
3. Sapp JL, Wells GA, Parkash R, et al. Ventricular tachycardia ablation versus escalation of antiarrhythmic drugs. N Engl J Med;375:111–121. [PubMed: 27149033]
4. Soejima K, Suzuki M, Maisel WH, et al. Catheter ablation in patients with multiple and unstable ventricular tachycardias after myocardial infarction: short ablation lines guided by reentry circuit isthmuses and sinus rhythm mapping. Circulation. 2001;104:664–669. [PubMed: 11489772]
5. Soejima K, Stevenson WG, Maisel WH, Sapp JL, Epstein LM. Electrically unexcitable scar mapping based on pacing threshold for identification of the reentry circuit isthmus: feasibility for guiding ventricular tachycardia ablation. Circulation. 2002;106:1678–1683. [PubMed: 12270862]
6. Bogun F, Good E, Reich S, et al. Isolated potentials during sinus rhythm and pace-mapping within scars as guides for ablation of post-infarction ventricular tachycardia. J Am Coll Cardiol. 2006;47:2013–2019. [PubMed: 16697318]
7. Cronin EM, Bogun FM, Maury P, et al. 2019 HRS/EHRA/APHRS/LHRS expert consensus statement on catheter ablation of ventricular arrhythmias. Heart Rhythm. 2020;17:e155–e205. [PubMed: 31102616]
8. Sapp JL, Bar-Tal M, Howes AJ, et al. Real-time localization of ventricular tachycardia origin from the 12-lead electrocardiogram. JACC Clin Electrophysiol. 2017;3:687–699. [PubMed: 29759537]
9. Prakosa A, Arevalo HJ, Deng D, et al. Personalized virtual-heart technology for guiding the ablation of infarct-related ventricular tachycardia. Nat Biomed Eng. 2018;2:732–740. [PubMed: 30847259]
10. Zhou S, Abdelwahab A, Horáček BM, et al. Prospective assessment of an automated intraprocedural 12-lead ECG-based system for localization of early left ventricular activation. Circ Arrhythm Electrophysiol. 2020;13:e008262. [PubMed: 32538133]
11. Asirvatham SJ, Stevenson WG. Expecting the expected: electrocardiographic identification for ablation targets. Circ Arrhythm Electrophysiol. 2016;9:e004726. [PubMed: 27956435]
12. Kemmelings JGC, Linnenbank AC, Muilwijk SLC, Sippensgroenewegen A, Peper A, Grimbergen CA. Automatic QRS onset and offset detection for body surface QRS integral mapping of ventricular tachycardia. IEEE Trans Biomed Eng. 1994;41:830–836. [PubMed: 7959810]
13. Arevalo HJ, Vadakkumpadan F, Guallar E, et al. Arrhythmia risk stratification of patients after myocardial infarction using personalized heart models. Nat Commun. 2016;7:11437. [PubMed: 27164184]
14. André Schmidt, Azevedo CF, Cheng A, et al. Infarct tissue heterogeneity by magnetic resonance imaging identifies enhanced cardiac arrhythmia susceptibility in patients with left ventricular dysfunction. Circulation. 2007;115:2006–2014. [PubMed: 17389270]
15. Bayer JD, Blake RC, Plank G, Trayanova NA. A novel rule-based algorithm for assigning myocardial fiber orientation to computational heart models. Ann Biomed Eng. 2012;40:2243–2254. [PubMed: 22648575]
16. Zhou S, Abdelwahab A, Sapp JL, Warren JW, Horáček BM. Localization of ventricular activation origin from the 12-lead ECG: a comparison of linear regression with non-linear methods of machine learning. Ann Biomed Eng. 2019;47:403–412. [PubMed: 30465152]

17. Hren R, Nenonen J, Horáček BM. Simulated epicardial potential maps during paced activation reflect myocardial fibrous structure. Ann Biomed Eng. 1998;26:1022–1035. [PubMed: 9846940]
18. Cuculich PS, Schill MR, Kashani R, et al. Noninvasive cardiac radiation for ablation of ventricular tachycardia. N Engl J Med. 2017;377:2325–2336. [PubMed: 29236642]
19. Tung R, Raiman M, Liao H, et al. Simultaneous endocardial and epicardial delineation of 3D reentrant ventricular tachycardia. J Am Coll Cardiol. 2020;75:884–897. [PubMed: 32130924]

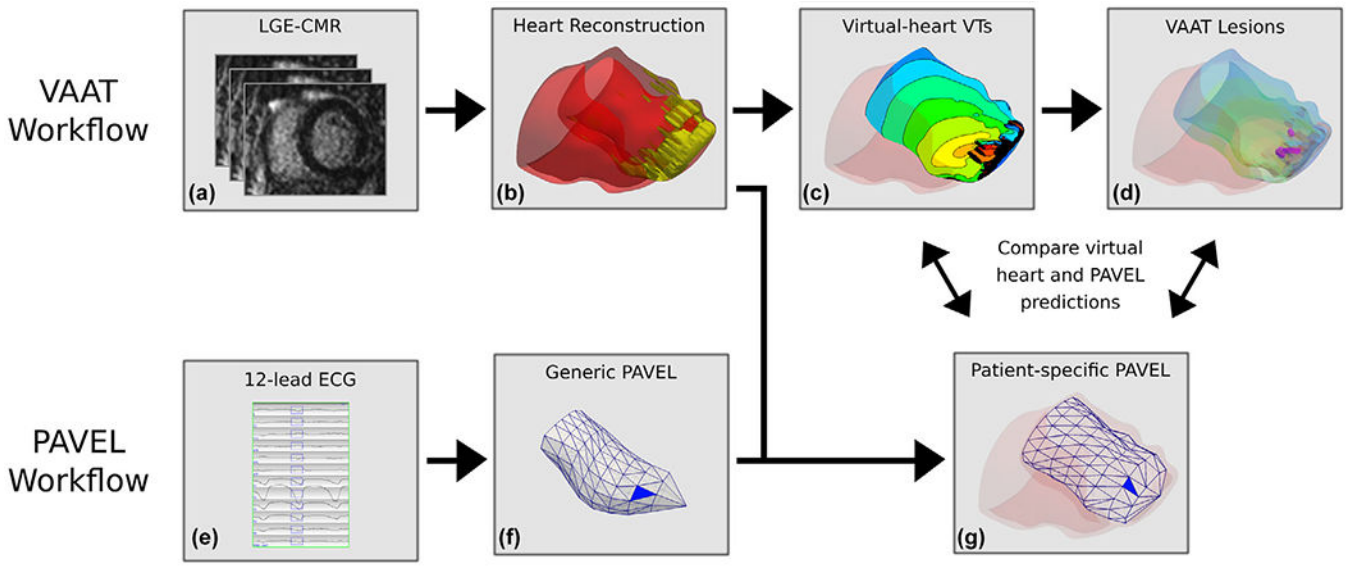

FIGURE 1.

Workflows of VAAT and PAVEL, and comparative analysis. VAAT Workflow: (A) From LGE-MRI stack for a patient, the myocardium is segmented into scar and grey zone tissues. (B) Personalized 3D virtual hearts are reconstructed from the segmented data and electrophysiological information is incorporated. (C) An endocardial activation map of the infarct-related VTs in a virtual heart. (D) VAAT-predicted ablation targets are marked by purple circles on the left ventricular endocardial surface. PAVEL Workflow: (E) The eight-lead ECGs of an induced monomorphic VT were recorded, and the other four leads (Lead III, aVF, aVL, aVR) were computed. The user can edit the onset of the 120 ms window (rectangle box) if correction is necessary. (F) A blue triangle that indicates the estimated VT exit location on a generic LV endocardial surface using PAVEL. (G) The PAVEL-predicted VT exit site on the generic LV endocardial surface was projected onto a patient-specific LV endocardial surface obtained from the personalized 3D digital heart. Comparative Analysis: we do not expect VAAT predicted ablation targets and PAVEL-predicted exit sites to necessarily co-localize; details in the text

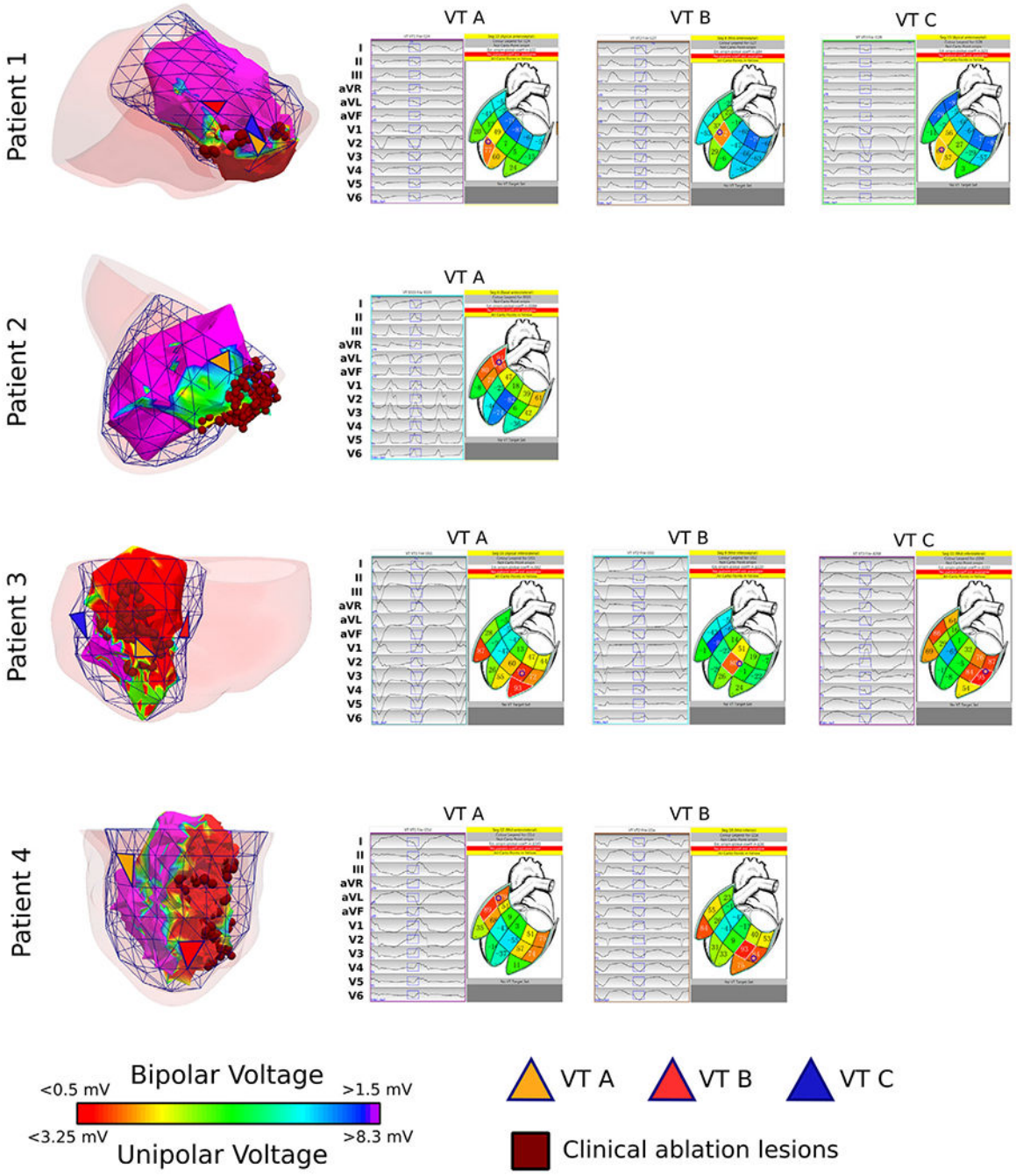

FIGURE 2.

Patient-specific PAVEL VT exit site predictions are concordant with clinical electroanatomic mapping (EAM) voltage maps. *Left*: The four patients' substrate voltage maps are shown together with the patient-specific PAVEL-predicted VT exit sites (orange, red, and blue triangles). All predicted VT exit sites localized near clinical ablation targets (dark red circles) and areas of border zone as defined by the bipolar voltage map between 0.5 mV and 1.5 mV (patients 1, 3 and 4) or unipolar voltage map between 3.25 mV and 8.3 mV (patient 2). *Right*: Screenshots of the PAVEL system graphical user interface are displayed. On the

left-hand side of each screenshot, the 12-lead ECG of the VT morphology is displayed (black traces) along with the 120-ms QRS integral window (blue rectangular boxes). This QRS integral window was used to localize the VT exit site. On the right-hand side of each screenshot, a 2D stylized LV endocardial surface is shown along with the predicted VT exit site (indicated by the bullseye)

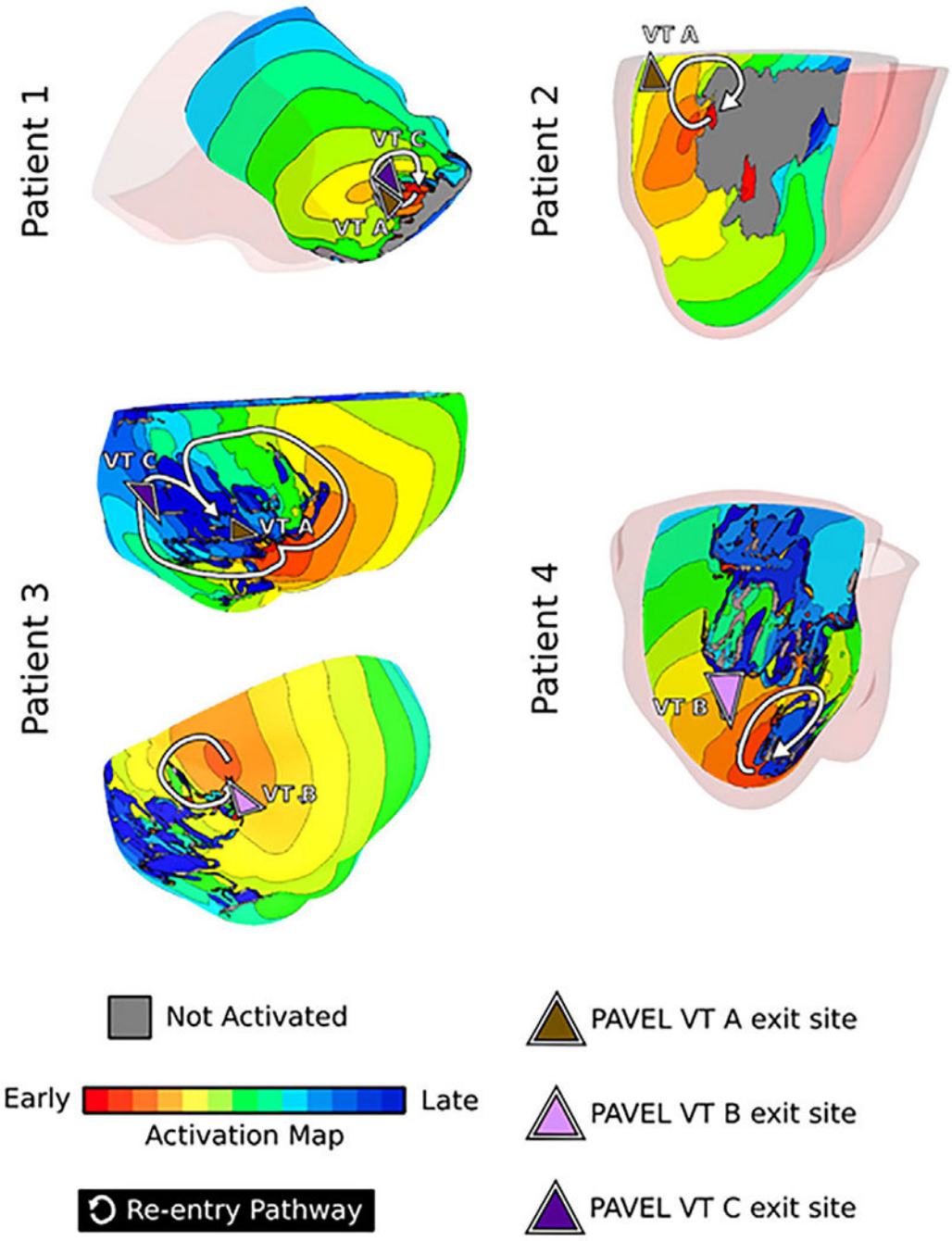

FIGURE 3.

Virtual-heart VT circuits correspond with PAVEL-predicted VT exit sites. Activation maps are shown for virtual-heart VT circuits that were proximal to PAVEL-VT exit site predictions. Brown, pink, and purple triangles denote the PAVEL-predicted VT A, B, and C exit sites, respectively; white arrows denote the re-entrant pathway

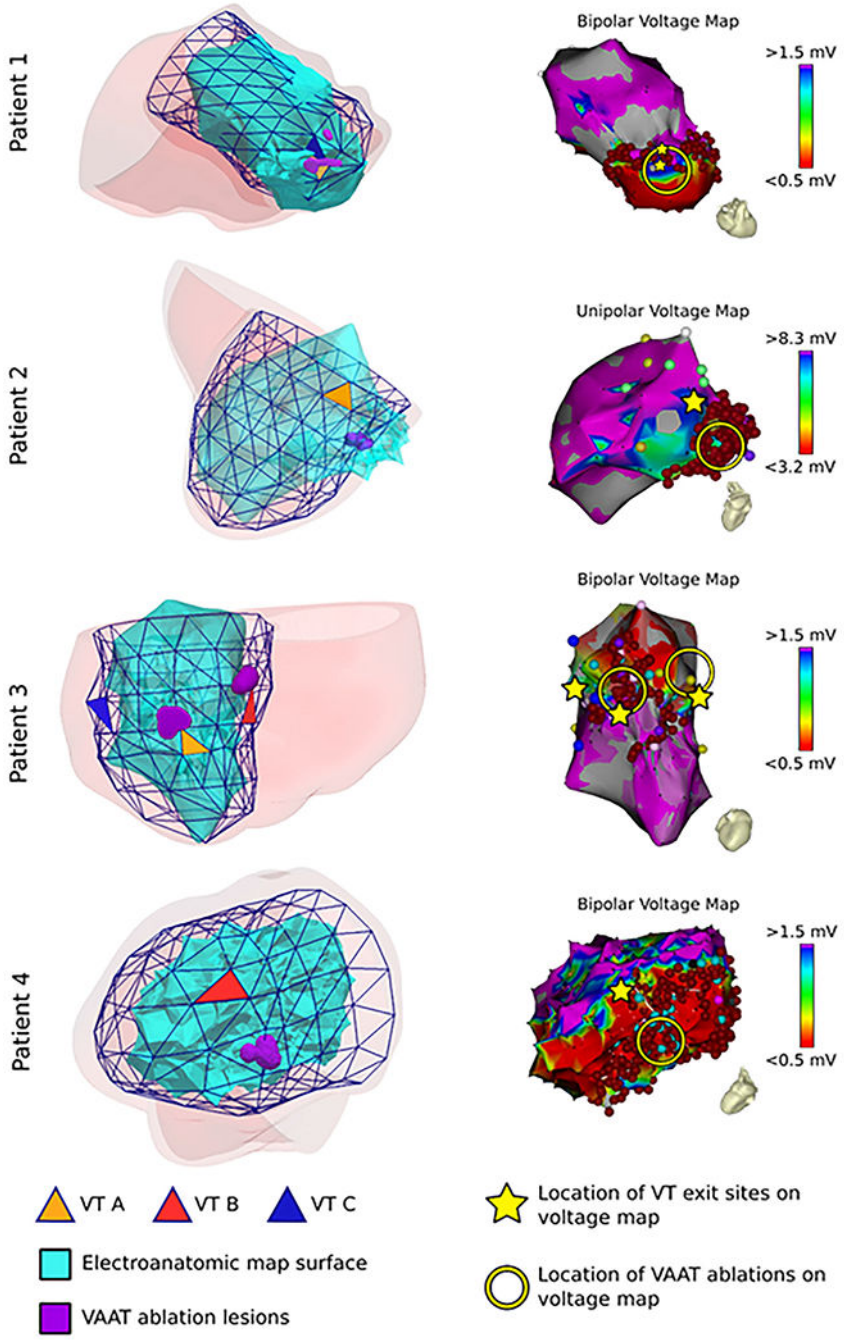

FIGURE 4.

VAAT targets are concordant with PAVEL-predicted VT exit sites. *Left*: The patient-specific PAVEL surfaces are shown along with the electroanatomic map surface, predicted VT exit sites (triangular elements), and VAAT ablations (purple). *Right*: The corresponding substrate voltage maps are shown. The VAAT ablations are shown in the yellow circle and PAVEL VT exit sites shown with the yellow star. For patient 4, fractionated potentials are shown in the light blue circles (bottom right panel)

TABLE 1

Baseline characteristics of patients enrolled in the study

Patient #	Sex	Age	Etiology	Mapped VT	Characteristics of VT morphology	ICD implanted	LVEF (%)	GZ (%)	Scar (%)
1	M	85	ICM	VTA	RB/Indeterminate axis/CL382 ms	YES	25	8.09	7.52
				VTB	RB/Inferior axis/CL365 ms				
				VTC	LB/Indeterminate axis/CL367 ms				
2	F	62	ICM	VTA	RB/ Inferior axis/CL260 ms	NO	60	4.74	7.43
3	M	59	ICM	VTA	RB/Superior axis/CL420 ms	YES	40	6.27	5.58
				VTB	LB/Superior axis/CL390 ms				
				VTC	RB/Superior axis/CL600 ms				
4	M	63	ICM	VTA	RB/Inferior axis/CL515 ms	YES	20	4.66	1.72
				VTB	RB/Superior axis/CL425 ms				
				VTC	RB/Inferior axis/CL370 ms				

Abbreviations: F, female; ICM, ischemic cardiomyopathy; LVEF, left ventricular ejection fraction. GZ (%), the percentage of the grey zone tissue of the LV; M, male; ms: milliseconds. Description of VT morphology: VT morphology/axis based on limb leads (superior axis (the QRS is negative in leads II, III, aVF), inferior axis (the QRS is positive in leads II, III, aVF))/cycle length (CL). ICD, implantable cardioverter-defibrillator; Scar (%), the percentage of the scar tissue of the LV.;VT, ventricular tachycardia. RB and LB refer to right bundle and left bundle.

TABLE 2

Summary of patient-specific PAVEL and VAAT predictions

Patient #	# of Triangles	Spatial resolution of triangular surface (cm^2)	Induced VT	Spatial resolution of the predicted VT exit site triangular areas (cm^2)	Virtual-heart VT circuits	Distance to nearest VAAT lesion (mm)
1	238	0.74	VTA	0.67	1	3.0
			VTB	0.48		–
			VTC	0.70		0.5
2	202	0.60	VTA	0.44	5	15.8
3	202	0.86	VTA	0.60	2	13.1
			VTB	0.96		13.0
			VTC	0.99		–
4	202	0.97	VTA	0.85	1	–
			VTB	1.09		18.9
			VTC	[a]N/A		–

[a]N/A identifies the predicted VT exit site was too basal to be localized onto the patient-specific LV endocardial surface.

"—" more details presented in the text.